Rapid Communications

Analysis of quantum effects inside spherical charged black holes

Assaf Lanir, Amos Ori, Noa Zilberman, Orr Sela, Ahron Maline, and Adam Levi
Department of Physics, Technion, Haifa 32000, Israel

(Received 8 November 2018; published 19 March 2019; corrected 27 May 2021)

We numerically compute the renormalized expectation value $\langle\hat{\Phi}^2\rangle_{\rm ren}$ of a minimally coupled massless quantum scalar field in the interior of a four-dimensional Reissner-Nordstrom black hole, in both the Hartle-Hawking and Unruh states. To this end we use a recently developed mode-sum renormalization scheme based on covariant point splitting. In both quantum states, $\langle\hat{\Phi}^2\rangle_{\rm ren}$ is found to approach a *finite* value at the inner horizon (IH). The final approach to the IH asymptotic value is marked by an inverse-power tail r_*^{-n}, where r_* is the Regge-Wheeler "tortoise coordinate" and with $n=2$ for the Hartle-Hawking state and $n=3$ for the Unruh state. We also report here the results of an analytical computation of these inverse-power tails of $\langle\hat{\Phi}^2\rangle_{\rm ren}$ near the IH. Our numerical results show very good agreement with this analytical derivation (for both the power index and the tail amplitude), in both quantum states. Finally, from this asymptotic behavior of $\langle\hat{\Phi}^2\rangle_{\rm ren}$ we analytically compute the leading-order asymptotic behavior of the trace $\langle\hat{T}^{\mu}_{\mu}\rangle_{\rm ren}$ of the renormalized stress-energy tensor at the IH. In both quantum states this quantity is found to diverge like $b(r-r_-)^{-1}r_*^{-n-2}$ (with n specified above and with a known parameter b). To the best of our knowledge, this is the first fully quantitative derivation of the asymptotic behavior of these renormalized quantities at the IH of a four-dimensional Reissner-Nordstrom black hole. In particular, this is the first conclusive result showing the divergence of the renormalized stress-energy tensor at the Cauchy horizon.

DOI: 10.1103/PhysRevD.99.061502

I. INTRODUCTION

Einstein's field equations admit black hole (BH) solutions endowed with remarkable exotic features including naked singularities, bridges to other universes and closed timelike curves. Among these solutions there is the Reissner-Nordstrom (RN) spacetime, describing a spherically symmetric BH carrying electric charge. This spacetime metric is given by

$$ds^2=-f(r)dt^2+\frac{1}{f(r)}dr^2+r^2(d\theta^2+\sin^2\theta d\varphi^2), \qquad (1)$$

where $f(r)=1-2M/r+Q^2/r^2$, M and Q being, respectively, the mass and charge of the BH. The event horizon (EH) and the inner horizon (IH) are, respectively, located at $r=r_+$ and $r=r_-$, the two solutions of $f(r)=0$ given by $r_\pm=M\pm(M^2-Q^2)^{1/2}$. Interestingly, this metric may be analytically continued through the BH interior into a concatenation of asymptotically flat spacetime regions ("other universes"), accessible to an observer in the "universe" where the BH originally formed only by traveling through the BH. Along the way through the BH and into the other universes, the observer must cross the IH that lies inside the BH. It is a treacherous path, however, as classical perturbations appear to form a null curvature singularity along the Cauchy horizon (CH) (the ingoing section of the IH). This is the situation in spherically symmetric charged BHs [1–6] as well as in spinning ones [7–9]. Nevertheless, this null singularity, caused by classical perturbing fields, is known to be weak [10] (i.e., tidally nondestructive [11], with a C^0 limiting metric)—in both the charged [3] and spinning [7,12] cases.

However, a general indication that emerges from a collection of analytical studies [13–15] on the effect of quantum perturbations inside BHs has been that semiclassical stress-energy fluxes are likely to diverge at the CH, although so far it remained inconclusive in four dimensions. It is the goal of this work to address this issue via concrete numerical calculation (augmented by some analytical results) of the actual strength and form of these quantum effects inside a charged BH.

Semiclassical gravity considers quantum matter fields propagating in a classical curved spacetime. The presence of curvature "deforms the vacuum" and induces a nontrivial stress energy in the quantum fields (even in "vacuum states"). In turn, this stress-energy tensor deforms the spacetime metric. This backreaction effect is to be determined from the semiclassical Einstein's field equation

$$G_{\mu\nu}=8\pi\langle\hat{T}_{\mu\nu}\rangle_{\rm ren}. \qquad (2)$$

Here $G_{\mu\nu}$ is the Einstein tensor of spacetime, and $\langle\hat{T}_{\mu\nu}\rangle_{\rm ren}$ is the renormalized stress-energy tensor (RSET) associated with the quantum fields.

For simplicity, our choice for a quantum field is that of a minimally coupled [16] massless scalar field, satisfying the

massless Klein-Gordon equation $\Box\hat{\Phi} = 0$, where $\hat{\Phi}$ is the scalar field operator and $\Box$ denotes the covariant d'Alembertian. It proves useful to first compute the renormalized vacuum expectation value $\langle\hat{\Phi}^2\rangle_{\rm ren}$ (often called the "vacuum polarization"), as it is simpler than the RSET but still captures many of its essential features and provides important insight into the physical content of different vacua. Furthermore, as will be seen below, the behavior of $\langle\hat{\Phi}^2\rangle_{\rm ren}$ actually determines the divergence rate of the RSET trace $\langle\hat{T}^{\mu}_{\mu}\rangle_{\rm ren}$ at the IH.

Semiclassical gravity predicts the evaporation of BHs through the emission of Hawking radiation [17,18]. BH evaporation obviously implies drastic differences in spacetime structure as compared to the corresponding classical picture. Likewise, it is conceivable that semiclassical stress-energy fluxes might affect the near-CH geometry inside RN (as well as Kerr) BHs more strongly than the classical perturbations do—potentially converting the CH into a strong (i.e., tidally destructive) spacelike singularity (and thereby preventing passage through the BH into the other universes). However, these issues remained unresolved and to address them one must, obviously, compute the RSET in the interior region of BHs and especially near the CH. We have therefore set out to ultimately compute the RSET in BH interiors, and we present here novel results for a first step in this direction: the numerical computation of $\langle\hat{\Phi}^2\rangle_{\rm ren}$ throughout the interior region [19] of a RN BH [20], followed by analysis of the leading-order behavior of $\langle\hat{\Phi}^2\rangle_{\rm ren}$ and also $\langle\hat{T}^{\mu}_{\mu}\rangle_{\rm ren}$ near the CH.

The renormalization of the divergent $\langle\hat{\Phi}^2\rangle$ was carried out here by the recently developed pragmatic mode-sum method [21,22], which numerically implements the point-splitting renormalization scheme developed by Christensen [23,24]. This prescription for $\langle\hat{\Phi}^2\rangle_{\rm ren}$ (and the same concept holds for $\langle\hat{T}_{\mu\nu}\rangle_{\rm ren}$ as well) is depicted in the following equation:

$$\langle\hat{\Phi}^2(x)\rangle_{\rm ren} = \lim_{x'\to x}[\langle\hat{\Phi}(x)\hat{\Phi}(x')\rangle - G_{\rm DS}(x,x')], \qquad (3)$$

where $G_{\rm DS}(x,x')$ is the DeWitt-Schwinger counterterm (explicitly given in [25]).

We consider here $\langle\hat{\Phi}^2\rangle_{\rm ren}$ in two quantum vacua. One is the Unruh state describing an evaporation of a BH [26], and the other is the Hartle-Hawking (HH) state describing a BH in thermal equilibrium [27,28] with an infinite bath of radiation. In Ref. [29] we derived an explicit expression for the scalar field two-point function in the RN interior, in both the Unruh and HH states, in terms of a radial function $\psi_{\omega l}(r)$ which can be computed numerically. This radial function satisfies the radial equation:

$$\frac{d^2\psi_{\omega l}}{dr_*^2} + [\omega^2 - V_l(r)]\psi_{\omega l} = 0, \qquad (4)$$

where ω denotes the mode's frequency (with respect to t) and l its angular-momentum number. Here the effective potential $V_l(r)$ is given by

$$V_l(r) = f(r)\left[\frac{l(l+1)}{r^2} + \frac{2M}{r^3} - \frac{2Q^2}{r^4}\right], \qquad (5)$$

and r_* is the tortoise coordinate defined by $dr/dr_* = f(r)$. Note that $r_* \to -\infty(+\infty)$ at the EH (IH). The boundary condition for $\psi_{\omega l}$ at the EH is

$$\psi_{\omega l} \cong e^{-i\omega r_*}, \qquad r_* \to -\infty. \qquad (6)$$

The required input for the computation of $\langle\hat{\Phi}^2\rangle_{\rm ren}$ inside the BH is the radial function $\psi_{\omega l}(r)$ and also $\rho^{\rm up}_{\omega l}$, namely the reflection coefficient for the "up" modes (see e.g., [29]) outside the BH. We compute $\psi_{\omega l}(r)$ and $\rho^{\rm up}_{\omega l}$ numerically and use them to construct the mode contributions to the two-point function inside the BH, as prescribed in Ref. [29]. Then we regularize the mode sum using the θ-splitting variant of our method, as described in [22]. This same method was implemented recently for computing $\langle\hat{\Phi}^2\rangle_{\rm ren}$ inside a Schwarzschild BH in Ref. [30], where a more detailed account of the procedure is provided. (Additional details are provided in Supplemental Material [31].)

From the symmetries of the RN geometry it immediately follows that $\langle\hat{\Phi}^2\rangle_{\rm ren}$ (like $\langle\hat{T}^{\mu}_{\mu}\rangle_{\rm ren}$) only depends on r. In the next section we present the results for $\langle\hat{\Phi}^2(r)\rangle_{\rm ren}$ throughout the range $r_- \le r \le r_+$. Interestingly, it turns out that for both the Unruh and HH states, $\langle\hat{\Phi}^2\rangle_{\rm ren}$ remains finite upon approaching the IH (although its gradient diverges there). Then subsequently we present analytical results for the asymptotic behaviors of $\langle\hat{\Phi}^2\rangle_{\rm ren}$ and $\langle\hat{T}^{\mu}_{\mu}\rangle_{\rm ren}$ very close to the IH, and for $\langle\hat{\Phi}^2\rangle_{\rm ren}$ we also compare our analytical and numerical results.

II. NUMERICAL RESULTS

We shall focus here on the specific example $Q/M = 0.8$. In this case $r_+ = 1.6M$ and $r_- = 0.4M$. The radial equation (4) together with the initial condition (6) was solved numerically for $\psi_{\omega l}(r)$, from the EH to very close to the IH, for a sufficiently dense set of ωl modes in the range $0 \le l \le 10$ and $0 < \omega < 10/M$. The reflection coefficient $\rho^{\rm up}_{\omega l}$ was also computed numerically for these ωl modes. These quantities were then used to construct $\langle\hat{\Phi}^2\rangle_{\rm ren}$. See Supplemental Material [31] for more details.

Figure 1 displays the numerical results for $\langle\hat{\Phi}^2(r)\rangle_{\rm ren}$ in the region between the two horizons (specifically for $0.5 \le r/M \le 1.6$), for both quantum states. Our result for the HH state agrees very nicely with the known analytical result [32,33] at the EH, with a difference of only $\sim$0.005%.

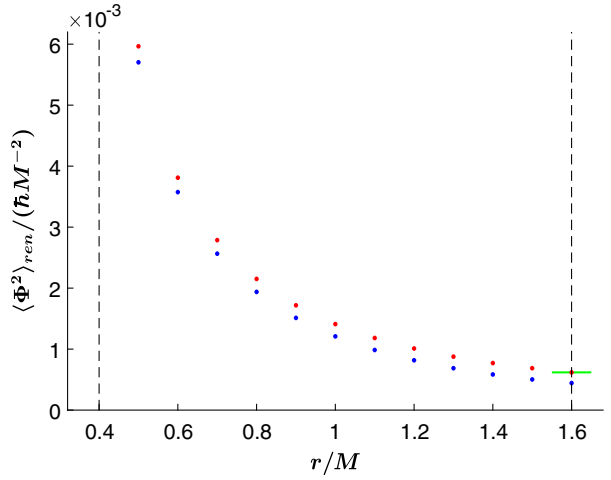

FIG. 1. The numerically computed $\langle\hat{\Phi}^2(r)\rangle_{\rm ren}$ in the HH (red) and Unruh (blue) states in the region between the two horizons. The short horizontal green line represents the analytical result for $\langle\hat{\Phi}^2(r)\rangle_{\rm ren}$ in the HH state at the EH.

The most obvious feature seen in this figure is the steady growth with decreasing r, which becomes steeper when getting close to the IH. This trend of sharp increase towards the IH continues all the way up to, say, $r - r_- \sim 10^{-6}M$. From this behavior one might get the impression (as we originally did) that $\langle\hat{\Phi}^2(r)\rangle_{\rm ren}$ would diverge at the IH.

To our surprise, we found that this picture drastically changes once we start exploring regions much closer to the IH. In fact, $\langle\hat{\Phi}^2(r)\rangle_{\rm ren}$ eventually approaches a *finite* value at $r \to r_-$, which we denote by $(\hbar/M^2)\langle\hat{\Phi}^2\rangle_-$, where the index "−" refers to the limit $r \to r_-$. This is clearly seen in Fig. 2, which displays $\langle\hat{\Phi}^2\rangle_{\rm ren}$ as a function of the logarithmic variable z defined by

$$z \equiv \ln(\delta r), \qquad \delta r \equiv (r - r_-)/M. \tag{7}$$

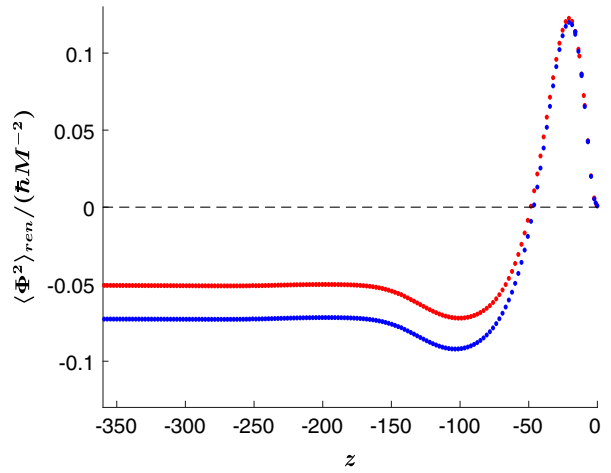

FIG. 2. $\langle\hat{\Phi}^2(r)\rangle_{\rm ren}$ in the HH (red) and Unruh (blue) states, as a function of z.

Note that the IH corresponds to $z \to -\infty$. In both quantum states, after a few quickly decaying oscillations (there are actually two maxima and two minima overall, although not all of them can be seen in this figure), $\langle\hat{\Phi}^2\rangle_{\rm ren}$ approaches a plateau. The asymptotic values are $\langle\hat{\Phi}^2\rangle_-^H \cong -0.05058$ and $\langle\hat{\Phi}^2\rangle_-^U \cong -0.07258$. Hereafter, an index "H" or "U" will denote the HH state or Unruh state, respectively.

III. NEAR-IH ASYMPTOTIC BEHAVIOR

To explore the near-IH asymptotic behavior we define (respectively, for each quantum state)

$$\Delta \equiv (M^2/\hbar)\langle\hat{\Phi}^2\rangle_{\rm ren} - \langle\hat{\Phi}^2\rangle_- \tag{8}$$

(i.e., the dimensionless deviation from $\langle\hat{\Phi}^2\rangle_-$).

As it turns out, $\Delta(z)$ decays like z^{-n}, where hereafter n will stand for either $n_H = 2$ (HH state) or $n_U = 3$ (Unruh state). To demonstrate this, Fig. 3 displays $z^n \cdot \Delta(z)$. The flat horizontal forms of the red and blue lines, at the left half of the z axis, clearly indicate this leading-order behavior $\Delta \propto z^{-n}$ in the two quantum states. (This behavior is seen even more clearly in Fig. 4.)

The effective potential $V_l(r)$, given in (5), vanishes at the IH like $f \propto \delta r$. Therefore, for sufficiently small δr the radial equation (4) becomes free, and its general solution in that domain is

$$\psi_{\omega l} \cong A_{\omega l}e^{i\omega r_*} + B_{\omega l}e^{-i\omega r_*} \quad (\delta r \ll 1). \tag{9}$$

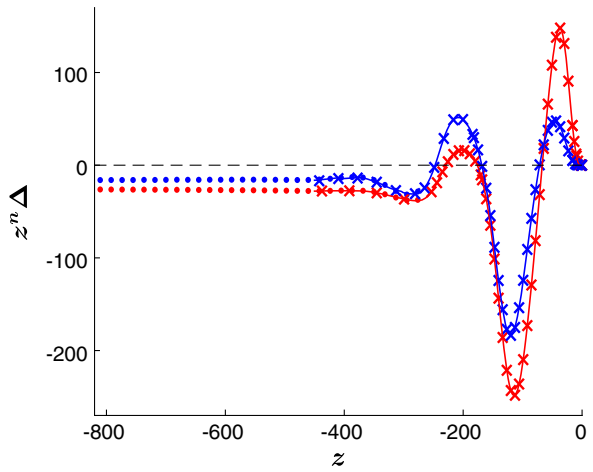

FIG. 3. $\Delta(z) \cdot z^n$ in the HH (red) and Unruh (blue) states, in the region $-845 < z < 0$ (which roughly corresponds to $10^{-367} < \delta r < 1$). The results for the Unruh state are divided here by a factor of -150, for convenience. The plateaus at the left half of the z axis indicate the inverse-power behavior $\Delta \propto z^{-n}$. For both the HH and Unruh results, the crosses indicate full numerical results, the solid curves indicate semiasymptotic results, and the dots indicate the "refined variant" results.

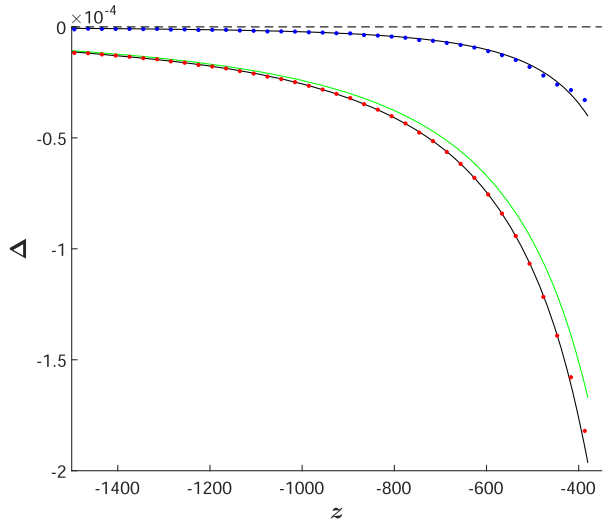

FIG. 4. $\Delta(z)$ in the HH state (red dots) and Unruh state (blue dots) exceedingly close to r_- (up to $z \sim 1500$, which roughly corresponds to $\delta r \sim 10^{-650}$), computed using the refined variant. The black curves are the analytical expressions (10) for the inverse-power tails. The green curve indicates the leading-order analytical result $\Delta_H \approx C_H z^{-2}$ (whereas the corresponding black curve also includes the next-order term $C_H^1 z^{-3}$).

The coefficients $A_{\omega l}$ and $B_{\omega l}$ are dictated by the scattering problem off the potential $V_l(r)$ from the EH to the IH and can be determined numerically. Note that on approaching the IH r_* diverges as $r_* \approx -z/2\kappa_-$, where $\kappa_- = (r_+ - r_-)/2r_-^2$ is the IH surface gravity.

In order to explore the aforementioned inverse-power decay we need to push the numerical solution to extremely small δr values, say $\delta r < e^{-400} \sim 10^{-175}$, as can be seen in e.g., Fig. 3. This is hard to do with the brute-force numerical solution for $\psi_{\omega l}$. [One of the difficulties, already seen in Eq. (9), is the very rapid variation of $\psi_{\omega l}$ with ω for $r_*/M \gg 1$.] To overcome this difficulty, we introduce the *semiasymptotic* approximation, in which we simply employ Eq. (9) as an approximation to $\psi_{\omega l}$ for sufficiently small δr. The results obtained from this approximation are displayed in Fig. 3 by the red and blue solid curves.

Still, in the deep tails region (say $z < -700$) even this semiasymptotic approximation starts to be noisy (when numerically implemented to explore the inverse-power tails). We therefore designed a refined variant of this approximation, aimed to explore the tails region, which can more efficiently take us to very large $|z|$ values. It is this refined variant that we have used to produce Fig. 4 below (and also the left region in Fig. 3). We point out that there are nice overlap regions on the z axis between these three slightly different numerical procedures, as may be seen e.g., in Fig. 3. This is further discussed in Supplemental Material [31], which provides additional information about the semiasymptotic approximation and its refined variant.

IV. ANALYTICAL EXPRESSIONS FOR THE INVERSE-POWER TAILS

To our pleasant surprise, we found that it is possible to obtain, analytically [34], the dominant inverse-power tails characterizing the near-IH asymptotic behavior of $\Delta(z)$. This is possible because, as it turns out, these tails are actually governed by the small-ω asymptotic behavior of $A_{\omega l}$, $B_{\omega l}$, and $\rho^{\rm up}_{\omega l}$; and this small-ω behavior can be deduced analytically. This analysis yields the two dominant inverse powers ($n_H = 2$ and $n_U = 3$) as well as their multiplicative amplitude parameters (for both quantum states).

Furthermore, since we had to carry the analysis to order z^{-3} (needed for the Unruh-state leading order), we actually got, almost for free, the term $\propto z^{-3}$ for the HH state as well. Thus, including all the inverse-power terms to which we presently have analytical access, we write the tail expressions as

$$\Delta_U = C_U z^{-3} + \cdots, \qquad \Delta_H = C_H z^{-2} + C_H^1 z^{-3} + \cdots, \tag{10}$$

where "$\cdots$" denotes higher-order corrections. Defining $\alpha \equiv r_+/r_-$, we find

$$C_U = 2\Lambda(1-\alpha^4)(1-\alpha)^2(11+14\alpha+11\alpha^2), \tag{11}$$

$$C_H = 3\Lambda\alpha^{-2}(1-\alpha^4)^2, \tag{12}$$

$$C_H^1 = 2\log\left[\frac{2(\alpha-1)}{\alpha+1}\right]C_H - \frac{1}{4}(\alpha^{-2}-3)C_U, \tag{13}$$

where $\Lambda \equiv (1-\alpha^2)/768\pi^2$.

Figure 4 displays the analytical expressions (10) (black curves) and the numerical data (dots) for the inverse-power tails, for both quantum states, in the range $400 < -z < 1500$. It shows excellent agreement, supporting the validity and accuracy of both the theoretical analysis and numerics.

V. TRACE OF THE STRESS TENSOR

For a minimally coupled massless scalar field, the RSET trace $\langle\hat{T}^\mu_\mu\rangle_{\rm ren}$ is uniquely determined [29] by $\langle\hat{\Phi}^2(x)\rangle_{\rm ren}$ via

$$\langle\hat{T}^\mu_\mu\rangle_{\rm ren} = -\frac{1}{2}\Box\langle\hat{\Phi}^2(x)\rangle_{\rm ren} + (\text{local term}). \tag{14}$$

The local term only depends on the background metric, which is perfectly regular at the IH. Therefore the singular piece of $\langle\hat{T}^\mu_\mu\rangle_{\rm ren}$ is fully described by the d'Alembertian term. Since the constant $\langle\hat{\Phi}^2\rangle_-$ contributes nothing to the d'Alembertian, we are left with $-(\hbar/2M^2)\Box\Delta$. Applying the d'Alembertian operator to Eq. (10), we obtain for the two quantum states, at leading order in $1/z$ (and δr),

$$\langle \hat{T}^{\mu}_{\mu} \rangle_{\rm ren} \cong n(n+1)\frac{\hbar}{M^2}\kappa_- \frac{C}{r-r_-} z^{-n-2}, \qquad (15)$$

where, recall, $n_H = 2$, $n_U = 3$ and C is either C_H or C_U specified above.

VI. DISCUSSION

We found that $\langle \hat{\Phi}^2 \rangle_{\rm ren}$ is finite at the IH. This finite asymptotic value is approached via a few quickly decaying oscillations followed by an inverse-power tail. In turn, the RSET trace $\langle \hat{T}^{\mu}_{\mu} \rangle_{\rm ren}$ diverges as $1/(r-r_-)$ softened by a certain inverse power of $\ln(r-r_-)$. We obtained a fully analytical description of this divergent trace (at leading order), Eq. (15). Obviously the divergence of the trace $\langle \hat{T}^{\mu}_{\mu} \rangle_{\rm ren}$ implies the divergence of the tensor $\langle \hat{T}_{\mu\nu} \rangle_{\rm ren}$. This is the first conclusive result showing the RSET divergence at the CH.

Here we only investigated numerically the case $Q/M = 0.8$. However, our results for the inverse-power tails—and, more importantly, for the asymptotic divergence (15) of the RSET trace—apply to any (nonextremal) M and Q.

The behavior of $\langle \hat{\Phi}^2 \rangle_{\rm ren}$ on approaching the IH is remarkably complex. In particular, the final inverse-power tails are only exposed at, say, $\delta r < 10^{-175}$. This complex asymptotic behavior may be traced to the factors $e^{\pm i\omega r_*}$ in Eq. (9). The mode contribution to $\langle \hat{\Phi}^2 \rangle_{\rm ren}$ contains terms quadratic in $\psi_{\omega l}$, including factors $e^{\pm 2i\omega r_*}$ (multiplying certain functions of $A_{\omega l}$, $B_{\omega l}$, etc.). Integration over ω then leaves a nontrivial function of r_*, embodied in the asymptotic behavior of $\langle \hat{\Phi}^2 \rangle_{\rm ren}$.

It is interesting to compare these results to a recent work [35] carried out by one of us (O. S.), in which the large-l approximation was used to obtain bounds on the divergence rate of $\langle \hat{\Phi}^2 \rangle_{\rm ren}$, $\langle \hat{T}^{\mu}_{\mu} \rangle_{\rm ren}$, and certain components of $\langle \hat{T}_{\mu\nu} \rangle_{\rm ren}$. In particular it was found that for both the Unruh and HH states $\langle \hat{\Phi}^2 \rangle_{\rm ren}$ and $\langle \hat{T}^{\mu}_{\mu} \rangle_{\rm ren}$ must be less divergent than $1/(r-r_-)$ and $1/(r-r_-)^2$, respectively. The results presented here for these two quantities are fully consistent with these bounds.

The expressions presented here for the prefactors C_H and C_U that control the divergence of $\langle \hat{T}^{\mu}_{\mu} \rangle_{\rm ren}$ only apply to a minimally coupled massless scalar field. In the case of nonminimal coupling they will change. In particular, in the case of conformal coupling these prefactors will vanish altogether, because the standard trace-anomaly formula guarantees regularity of the trace at the IH. The same situation will occur in the case of a quantum electromagnetic field, since this field is conformal too.

It is still unclear, however, if the *gravitational* semiclassical contribution to the effective stress energy will possess such a trace divergence at the IH. The presence of a gravitational contribution (associated with quantized linearized modes of the gravitational field) to the effective $\langle \hat{T}_{\mu\nu} \rangle_{\rm ren}$ is obvious from the very basic fact that gravitons do significantly contribute to Hawking radiation [36] (and, correspondingly, negative semiclassical gravitational-field influx must penetrate into the EH of the evaporating BH and contribute to its shrinkage). However, a formalism for quantifying the semiclassical effective gravitational stress-energy tensor has not been formulated so far.

This analysis calls for extension in several obvious directions. The first obvious step is to elevate the analysis from $\langle \hat{\Phi}^2 \rangle_{\rm ren}$ to the RSET. Second, the quantum scalar field should better be replaced by the (more realistic) quantum electromagnetic field. In addition, it will be important to extend the analysis from RN to the Kerr background (a spinning BH), which is obviously much more realistic than a spherical charged BH.

Finally, it will be very interesting (but also very challenging) to explore the backreaction effect of the semiclassical RSET on the BH interior, according to the semiclassical Einstein equation (2).

ACKNOWLEDGMENTS

We thank Robert Wald, Marc Casals, and Adrian Ottewill for interesting and helpful discussions. This research was supported by the Asher Fund for Space Research at the Technion. The work of A. L. and O. S. was further supported by the Israel Science Foundation under Grant No. 1696/15 and by the I-CORE Program of the Planning and Budgeting Committee. The work of N. Z. was partly supported by the Israel Science Foundation under Grant No. 600/18.

[1] W. A. Hiscock, Evolution of the Interior of a Charged Black Hole, Phys. Rev. Lett. **83**, 110 (1981).
[2] E. Poisson and W. Israel, Internal structure of black holes, Phys. Rev. D **41**, 1796 (1990).
[3] A. Ori, Inner Structure of a Charged Black Hole: An Exact Mass-Inflation Solution, Phys. Rev. Lett. **67**, 789 (1991).
[4] P. R. Brady and J. D. Smith, Black Hole Singularities: A Numerical Approach, Phys. Rev. Lett. **75**, 1256 (1995).
[5] S. Hod and T. Piran, Mass Inflation in Dynamical Gravitational Collapse of a Charged Scalar Field, Phys. Rev. Lett. **81**, 1554 (1998).
[6] L. M. Burko, Structure of the Black Hole's Cauchy-Horizon Singularity, Phys. Rev. Lett. **79**, 4958 (1997).

[7] A. Ori, Structure of the Singularity Inside a Realistic Rotating Black Hole, Phys. Rev. Lett. **68**, 2117 (1992).
[8] P. R. Brady, S. Droz, and S. M. Morsnik, Late-time singularity inside nonspherical black holes, Phys. Rev. D **58**, 084034 (1998).
[9] A. Ori, Oscillatory Null Singularity Inside Realistic Spinning Black Holes, Phys. Rev. Lett. **83**, 5423 (1999).
[10] F. J. Tipler, Singularities in conformally flat spacetimes, Phys. Lett. **64A**, 8 (1977).
[11] A. Ori, Strength of curvature singularities, Phys. Rev. D **61**, 064016 (2000).
[12] M. Dafermos and J. Luk, The interior of dynamical vacuum black holes I: The C^0-stability of the Kerr Cauchy horizon, arXiv:1710.01722.
[13] N. D. Birrell and P. C. W. Davies, On falling through a black hole into another universe, Nature (London) **272**, 35 (1978).
[14] A. C. Ottewill and E. Winstanley, Renormalized stress tensor in Kerr space-time: General results, Phys. Rev. D **62**, 084018 (2000).
[15] W. A. Hiscock, Quantum-mechanical instability of the Kerr-Newman black-hole interior, Phys. Rev. D **21**, 2057 (1980).
[16] The results described below for $\langle\hat{\Phi}^2\rangle_{\rm ren}$ are actually independent of the coupling constant (because the Ricci scalar vanishes in our case). However, the results for $\langle\hat{T}^{\mu}_{\mu}\rangle_{\rm ren}$ only apply for a minimally coupled field.
[17] S. W. Hawking, Black hole explosions, Nature (London) **248**, 30 (1974).
[18] S. W. Hawking, Particle creation by black holes, Commun. Math. Phys. **43**, 199 (1975).
[19] Throughout, by "interior region" we actually refer to the "predictable" internal domain $r_- \leq r \leq r_+$.
[20] We shall consider here a fixed RN geometry, without backreaction.
[21] A. Levi and A. Ori, Pragmatic mode-sum regularization method for semiclassical black-hole spacetimes, Phys. Rev. D **91**, 104028 (2015).
[22] A. Levi and A. Ori, Mode-sum regularization of $\langle\phi^2\rangle$ in the angular-splitting method, Phys. Rev. D **94**, 044054 (2016).
[23] S. M. Christensen, Vacuum expectation value of the stress tensor in an arbitrary curved background: The covariant point separation method, Phys. Rev. D **14**, 2490 (1976).
[24] S. M. Christensen, Regularization, renormalization, and covariant geodesic point separation, Phys. Rev. D **17**, 946 (1978).
[25] P. R. Anderson, W. A. Hiscock, and D. A. Samuel, Stress-energy tensor of quantized scalar fields in static spherically symmetric spacetimes, Phys. Rev. D **51**, 4337 (1995).
[26] W. G. Unruh, Notes on black-hole evaporation, Phys. Rev. D **14**, 870 (1976).
[27] J. B. Hartle and S. W. Hawking, Path-integral derivation of black-hole radiance, Phys. Rev. D **13**, 2188 (1976).
[28] W. Israel, Thermo-field dynamics of black holes, Phys. Lett. **57A**, 107 (1976).
[29] A. Lanir, A. Levi, A. Ori, and O. Sela, Two-point function of a quantum scalar field in the interior region of a Reissner-Nordstrom black hole, Phys. Rev. D **97**, 024033 (2018).
[30] A. Lanir, A. Levi, and A. Ori, Mode-sum renormalization of $\langle\hat{\Phi}^2\rangle$ for a quantum scalar field inside a Schwarzschild black hole, Phys. Rev. D **98**, 084017 (2018).
[31] See Supplemental Material at http://link.aps.org/supplemental/10.1103/PhysRevD.99.061502 for a terse presentation of the methods used to generate the three variants of results, as well as the specific numerical parameters we chose.
[32] V. P. Frolov, Vacuum polarization near the event horizon of a charged rotating black hole, Phys. Rev. D **26**, 954 (1982).
[33] A. Ottewill (private communication).
[34] A. Maline *et al.* (to be published).
[35] O. Sela, Quantum effects near the Cauchy horizon of a Reissner-Nordstrom black hole, Phys. Rev. D **98**, 024025 (2018).
[36] D. N. Page, Particle emission rates from a black hole: Massless particles from an uncharged, nonrotating hole, Phys. Rev. D **13**, 198 (1976).

Correction: The previously published Fig. 4 contained colored dots that were inconsistent with labeling in the caption and has been replaced.